

# Using sentinel-2 satellite imagery to develop microphytobenthos-based water quality indices in estuaries

Simon Oiry, Laurent Barillé\*

Université de Nantes, Laboratoire Mer Molécules Santé (EA 2160), Faculté des Sciences et des Techniques, BP 92208, 44322 Nantes Cedex 3, France

## ARTICLE INFO

### Keywords:

Benthic algae  
Estuary  
Microphytobenthos  
Sentinel-2  
Water Framework Directive

## ABSTRACT

Microphytobenthos (MPB) is composed of unicellular photosynthetic organisms that colonize intertidal sediments within the first millimeters of the photic zone and form biofilms at low tide. In estuaries, this benthic group can represent the main primary producer and deliver several ecosystem services. However, it is not currently used as a bioindicator of water quality, contrary to the widespread use of phytoplankton in freshwater settings. This study assesses the potential of developing MBP metrics to assess water quality in transitional waters using Sentinel-2 (S2) satellite imagery. A Random Forest machine learning classification was used to distinguish different types of intertidal vegetation in 26 French estuaries and bays, in particular MPB and green macroalgae (chlorophytes), using multispectral indices. High accuracy was generally achieved for the identification of MPB when compared with field validation data, for both User's and Producer's accuracies, which corresponded to 94% and 84% respectively. Two Earth observation variables were retrieved: the Normalized Difference Vegetation Index (NDVI), a proxy of MPB biomass, and MPB percent cover integrated over the entire intertidal area of the water body. From a total of 918 S2 images from over a full year, 28% were exploitable due to the combined requirements of cloud-free pixels collected during low tide. With its 10 m spatial resolution, S2 was able to map all estuaries. MPB percent cover showed a stronger gradient between estuaries than MPB NDVI. MPB percent cover was also significantly correlated with green macroalgae percent cover, and a group of estuaries characterized by the highest MPB and green macroalgae coverage corresponded to eutrophic sites impacted by intensive farming activities. A multivariate analysis confirmed that MPB percent cover was indeed related to nutrients. It was also related to sediment type which was one of the main factors underlying differences between estuaries. This work is a first step toward a water quality metric using MPB, and several recommendations are proposed to refine this approach. Sentinel-2 imagery, which is publicly available, presents an interesting compromise to map estuarine microphytobenthos in order to assess the ecological status of transitional waters.

## 1. Introduction

Estuaries are among the most productive aquatic ecosystems and provide numerous services, including nutrient cycling, nurseries for commercial species, shoreline stabilization, protection from floods, and buffering against sea-level rise (Barbier et al., 2011; McLusky and Elliott, 2004). However, as coastal areas, they are heavily used and threatened by intense anthropogenic pressures, and affected by multiple drivers (Halpern et al., 2008; Merrifield et al., 2011). In Europe, the Water Framework Directive (WFD) establishes a framework for the protection of coastal and transitional waters (estuaries and lagoons) (European Commission, 2000). The ecological status of water bodies is based on hydromorphological, physico-chemical, and biological elements (Borja

et al., 2013). Biological water quality metrics are based on the presence and abundance of fish, macroinvertebrates, macroalgae, seagrass, and phytoplankton. Phytoplankton is the most reported indicator in lakes and coastal waters, but for 57% of transitional waters, its status is "unknown" (European Environment Agency, 2018). In turbid estuaries, phytoplankton metrics developed for coastal areas are not applicable. Light attenuation by suspended particulate matter limits phytoplankton production (Cloern, 1987) despite high nutrient concentration (Monbet, 1992). There is, however, another group of ubiquitous unicellular primary producers that contributes significantly to estuarine productivity: intertidal microphytobenthos (MPB); (Consalvey et al., 2004; Frankenbach et al., 2020; Underwood and Kromkamp, 1999). Intertidal MPB refers to unicellular microalgae and cyanobacteria

\* Corresponding author.

E-mail address: [Laurent.Barille@univ-nantes.fr](mailto:Laurent.Barille@univ-nantes.fr) (L. Barillé).

<https://doi.org/10.1016/j.ecolind.2020.107184>

Received 19 June 2020; Received in revised form 5 November 2020; Accepted 12 November 2020

Available online 28 November 2020

1470-160X/© 2020 The Authors.

Published by Elsevier Ltd.

This is an open access article under the CC BY-NC-ND license

(<http://creativecommons.org/licenses/by-nc-nd/4.0/>).

colonizing superficial sediments. Diatoms are usually the dominant microalgal component of MPB communities in intertidal estuarine and coastal areas (MacIntyre et al., 1996).

MPB is not used by the WFD as a biological indicator (Brito et al., 2010), and its potential as a biological quality indicator has been underinvestigated (Trobajo and Sullivan, 2010). In fact, the Directive only recognizes phytobenthos (benthic algae) in reference to freshwater organisms (Kelly, 2013). Many freshwater quality indices are based on diatom taxonomic composition (Prygiel and Coste, 1993), but there are no such indices for microphytobenthos. MPB is notoriously difficult to extract from the sediment and challenging to identify at a high taxonomic resolution (Ribeiro et al., 2020). On the other hand, MBP can grow biofilms covering several hectares of estuarine tidal flats (Benyoucef et al., 2014). These macroscale structures can be observed using satellite remote-sensing and quantified in terms of areal extent and biomass (Brito et al., 2013; Daggert et al., 2020; van der Wal et al., 2010). Most studies have used the Normalized Difference Vegetation Index (NDVI), which combines information at the red and near-infrared wavelengths (Tucker, 1979), as a proxy for benthic chlorophyll-*a* concentration (Barillé et al., 2011). Satellite imagery can, therefore, be a valuable tool to monitor estuarine water quality (Fichot et al., 2016; Mantas et al., 2013), but depends strongly on the spatial, temporal, and spectral resolutions (Muller-Karger et al., 2018). The MultiSpectral Instrument (MSI) aboard the European Space Agency Sentinel-2 (S2) satellite has a high 10 and 20 m spatial resolution that should allow estuaries to be mapped for satellite-derived water quality assessment (Schaeffer and Myer, 2020). With a constellation of twin satellites (S2A and S2B), the S2 mission also offers a high temporal resolution, with a revisit time of 5 days. The main constraint to discriminating MPB from

other intertidal vegetation is the limited number of spectral bands in the visible and the near-infrared range of S2 MSI (Drusch et al., 2012). With a multispectral NDVI, MPB may be confused with sparse macroalgae or seagrass (Barillé et al., 2010; Méléder et al., 2003a,b). The problem may, however, be overcome using machine learning classification techniques that have been successfully used to produce global maps of tidal flats (Murray et al., 2019) and to identify benthic vegetation using multi-spectral sensors (Traganos and Reinartz, 2018a,b). To our knowledge, machine learning classifiers, such as Support Vector Machine, *k*-Nearest Neighbor, and Random Forest (Zhang, 2015), have not yet been tested to discriminate MPB from other types of benthic vegetation.

In this study, we first want to test the suitability of S2 MSI imagery for mapping the distribution of microphytobenthos in French estuaries. We hypothesize that 1) the S2 spatial resolution is suited to mapping smaller estuaries with riverine morphology, and 2) the S2 spectral resolution allows MPB to be discriminated from macrophytes colonizing the intertidal zone. Physico-chemical data were collected to describe each estuary and we used Multidimensional Scaling (MDS) multivariate analysis to identify groups sharing common characteristics. Relationships between MPB and these environmental data were further explored with a redundancy analysis. Particular attention was paid to the sediment type, which is known to play a significant role in MPB distribution (Paterson and Hagerthey, 2001). Our main objective and the novelty of this work lies in the development of an estuarine water quality bio-indicator using intertidal surfaces colonized by MPB in twenty six contrasted sites. The strengths and limitations of S2 to derive MPB remotely-sensed metrics are discussed.

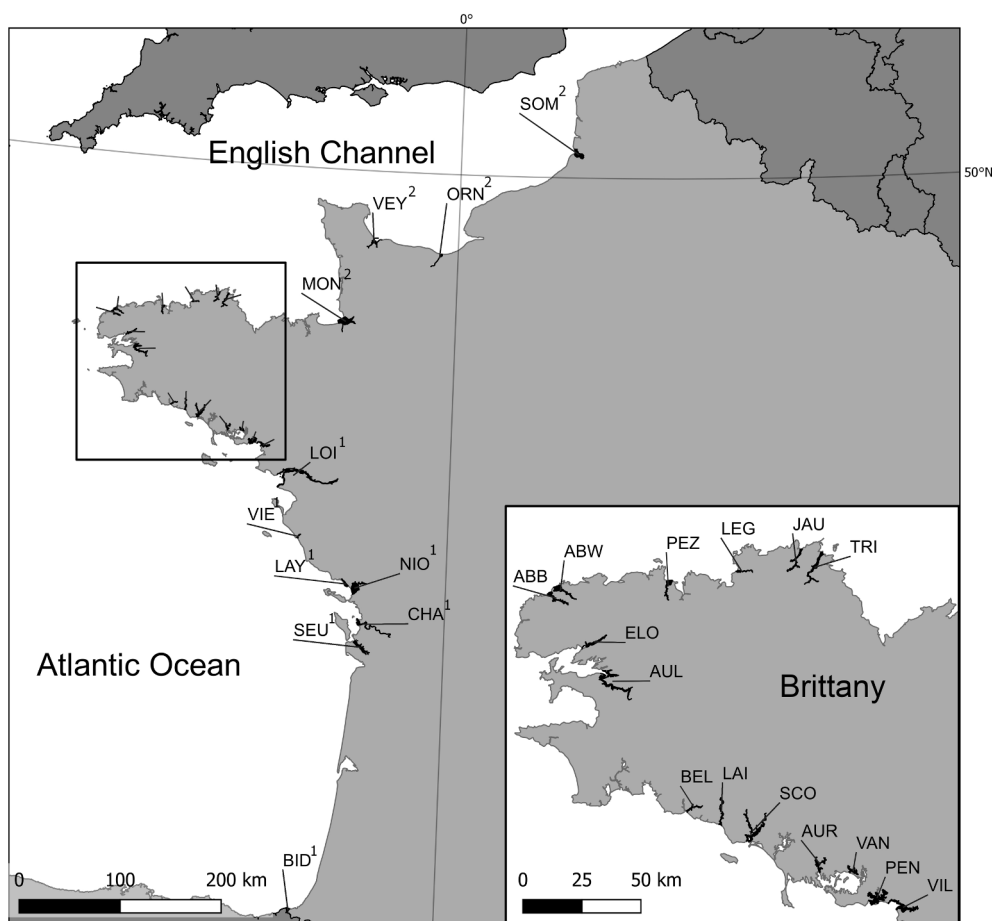


**Fig. 1.** Locations of the 26 study sites along the French coasts. Estuaries located in Brittany are detailed in the inset. Abbreviations are detailed in Table 1. All sites are Transitional Water Bodies according to the European Water Framework Directive.

## 2. Materials & methods

### 2.1. Study site

All study sites are estuaries (23) and bays (3) located along the French Atlantic coast and the English Channel (Fig. 1). They were categorized as belonging to either the Channel (CHA), Brittany (BRI), or to the southern part of the Bay of Biscay Atlantic coast (ATL). Estuaries in Brittany are generally smaller and are characterized by higher concentrations of nutrients originating from farming activities (Fig. 2, Ménesguen et al., 2018). Their catchment areas are dominated by agriculture, including significant livestock production. All sites have an intertidal zone with various tidal ranges and have been identified as Transitional Water Bodies (TWBs) by the French Biodiversity Agency in charge of implementing the European WFD (European Commission, 2000). Waterbody masks generated by this national agency were used to identify each TWB. In estuaries, they cover the oligo-, meso-, and polyhaline sections, which were considered together in this study. In some cases, such as Mont-Saint-Michel Bay, the TWB mask does not include the whole bay, but is instead restricted to the area below fluvial influence. The main characteristics of each site are provided in Table 1. Although there are 43 TWBs in France, we only considered those for which environmental data were available, notably sediment type.

### 2.2. Satellite data

A total of 918 Sentinel-2 images from January 1st to December 31st 2018 were downloaded from the Copernicus website (<https://scihub.copernicus.eu/dhus/#/home>). To download several images automatically, an R script was developed, using the *16EAGLE/GetSpatialData* R package. Ortho-rectified, geo-located, and radiometrically calibrated Level-2A data were used. Images were distributed as bottom-of-atmosphere reflectance with atmospheric correction performed using Sen2Cor (Main-Knorn et al., 2017). In a concurrent study carried out in Bourgneuf Bay (France) (Zoffoli et al., 2020), the performance of ESA's standard atmospheric correction was tested and found to be satisfactory for the study of intertidal vegetation. The dataset combined images from the two S2 satellites with different orbital cycles (#137 and #94), allowing a revisit time of 3–5 days. A preliminary selection was applied to all images with a relaxed constraint of less than 80% of cloud cover for the entire S2 tile. A subsequent selection considered clouds over the intertidal areas and low tide conditions (see Section 2.4). Four 10 m spatial resolution bands from the MSI sensor were used to calculate the multispectral indices: B2 (490 nm), B3 (560 nm), B4 (665 nm), and B8 (842 nm), as well as six bands with a 20 m spatial resolution; four in the near infrared (NIR), B5 (705 nm), B6 (740 nm), B7 (783 nm), and B8a (865 nm), and two in the shortwave infrared (SWIR), B11 (1610 nm) and B12 (2190 nm). All 20 m-resolution bands were resampled to 10 m using

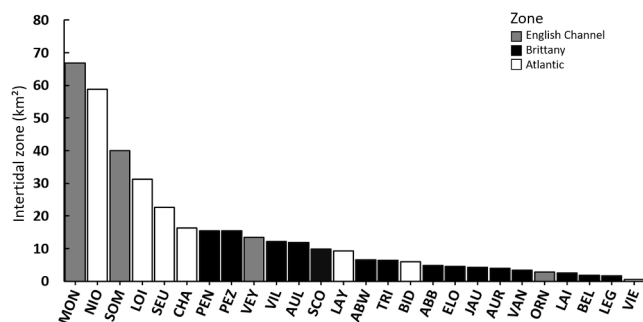


Fig. 2. Intertidal area (km<sup>2</sup>) of the 26 study sites distributed along the three main coastal zones: the English Channel, Brittany, and the southern part of the French Atlantic coast. Abbreviations are detailed Table 1. For each site, the area corresponds to the Transitional Water Body perimeter defined by the French Agency of Biodiversity.

the *Raster* package of R.

### 2.3. Random forest classification

One challenge of this study was to distinguish between different types of intertidal vegetation, in particular microphytobenthos from green macroalgae (chlorophytes), using multispectral indices. The other groups of plants that can be encountered in estuarine intertidal zones are brown macroalgae (pheophytes) and angiosperms. The main intertidal angiosperm is the seagrass, *Zostera noltei*. Terrestrial angiosperms from the schorre (uppermost intertidal level) can also be observed in the upper part of the intertidal zone. Although stranded red macroalgae (rhodophytes) can be observed locally, these were not considered in this study. Epiphytes colonizing macrophytes were also not considered, but do not interfere with the spectral discrimination between species (Fyfe, 2003). We therefore selected Random Forest (RF), a machine learning classification combining decision trees and bootstrapping (Breiman, 2001), which has successfully been used for tidal flats (Murray et al., 2019) and benthic vegetation (Traganos and Reinartz, 2018a,b). Applied to subtidal and intertidal seagrass, coral reefs, or coastal meadows, it was found to perform better than simpler classification algorithms and produced at least equivalent results to other machine learning classifiers, such as Support Vector Machine or *k*-Nearest Neighbor (Traganos and Reinartz, 2018a,b; Villoslada et al., 2020; Zhang, 2015). Random Forest uses supervised classification algorithms, which allows collinearity and non-linearity between predictive variables to be handled. Each decision tree is created using a random sample of predictive data, resampled at each iteration of the algorithm. Then, for each pixel, the final classification is obtained by a majority vote (the final class of a pixel is the class which appeared most often at the end of each algorithm iteration). This classification method can be divided into three steps: model building, image classification, and accuracy assessment (Fig. 3).

### 2.4. RF model building

Prior to classification, training was implemented using field measurements taken at low tide in May 2019, in the Penzé and Morlaix estuaries (Brittany) and in Bourgneuf Bay, south of the Loire estuary (Atlantic). Areas corresponding to the main types of benthic vegetation and substrates were delineated using a Garmin 60S GPS (Garmin Cooperation, Lenexa, Kansas, USA) with a spatial resolution of 3 m to create regions of interest (ROIs). In total, eight classes were created: sand, mud, water, brown algae, green algae, microphytobenthos, angiosperms from the schorre (uppermost intertidal level), and marine angiosperms (seagrass). A total of 113 polygons were randomly delineated in the field, with each polygon covering a minimum surface of six 20 m S2 pixels (Supplementary S3). An area-proportional allocation of training samples per class was carried out (Colditz, 2015). Reflectance data for all classes were obtained from quasi-synchronous S2 images. The RF model was created using the *Caret* package of R (Kuhn, 2008). Two parameters need to be set up: the number of trees ( $n_{tree}$ ) and the number of variables to be selected and tested for the best split when growing the trees ( $m_{try}$ ). The number of trees was set to 500 (Belgiu and Drăgu, 2016). A range from 250 to 1000 trees was tested in a previous step and showed that classification accuracy did not improve beyond 500. All 10 and 20 m (spatially resampled at 10 m) S2 bands mentioned previously were used as predictors. The other predictors were two multispectral indices used by Murray et al. (2019) for tidal flats: the NDVI and the Normalized Different Water Index (NDWI), and two additional vegetation indices, the Atmospherically Resistant Vegetation Index (ARVI) and the Modified Chlorophyll Absorption Ratio Index (MCARI) (Daughtry et al., 2000; Kaufman and Tanré, 1992; McFeeters, 1996; Rouse et al., 1973). Other indices, such as the Soil Adjusted Vegetation Index (SAVI) and the Enhanced Vegetation Index (EVI) have also been tested but were not implemented in the final model because

**Table 1**

Description of estuaries and bays identified as Transitional Water Bodies (TWB) by the French Biodiversity Agency in charge of the implementation of the Water Framework Directive. The tidal ranges cover different regimes: meso-tidal (1), macro-tidal (2), and mega-tidal (3).

Name	Code	Coordinates	Intertidal area (km <sup>2</sup> )	Mean tidal range (m)	Mud (% cover)	Number of images
Aber Benoit	ABB	48.56° – 4.59°	4.8	6.75 <sup>2</sup>	56	5
Aber Wrac'h	ABW	48.61° – 4.57°	6.58	6.75 <sup>2</sup>	98	5
Aulne	AUL	48.23° – 4.12°	11.84	6.15 <sup>2</sup>	100	4
Auray	AUR	47.63° – 2.95°	4.01	4.05 <sup>2</sup>	100	7
Belon	BEL	47.82° – 3.7°	1.77	4.15 <sup>2</sup>	99	15
Bidassoa	BID	43.37° – 1.78°	5.9	3.9 <sup>1</sup>	33	3
Charente	CHA	45.96° – 1.05°	25.37	5.2 <sup>2</sup>	98	4
Elorn	ELO	48.42° – 4.31°	4.59	6 <sup>2</sup>	100	6
Jaudy	JAU	48.77° – 3.23°	4.18	8.45 <sup>3</sup>	100	8
Laïta	LAI	47.85° – 3.53°	2.48	4.15 <sup>2</sup>	11	15
Lay	LAY	46.32° – 1.29°	9.24	5 <sup>2</sup>	100	20
Leguer	LEG	48.73° – 3.53°	1.61	7.85 <sup>2</sup>	51	7
Loire	LOI	47.29° – 2.1°	31.3	4.75 <sup>2</sup>	64	9
Mont Saint Michel	MON	48.62° – 1.49°	66.77	13.2 <sup>3</sup>	0	12
Sèvre Niortaise	NIO	46.27° – 1.14°	58.81	5.25 <sup>2</sup>	100	16
Orne	ORN	49.27° – 0.22°	2.76	6.7 <sup>2</sup>	0	17
Penerf	PEN	47.53° – 2.64°	15.37	4.7 <sup>2</sup>	94	7
Penzé	PEZ	48.64° – 3.95°	5.61	7.65 <sup>2</sup>	100	10
Scorff	SCO	47.75° – 3.31°	9.85	4.2 <sup>2</sup>	100	14
Seudre	SEU	45.79° – 1.14°	22.59	4.8 <sup>2</sup>	97	7
Somme	SOM	50.22° 1.58°	40.03	10.1 <sup>3</sup>	0	14
Trieux	TRI	48.77° – 3.11°	6.41	9.2 <sup>3</sup>	100	8
Vannes	VAN	47.63° – 2.76°	3.42	2.7 <sup>1</sup>	100	8
Veys	VEY	49.37° – 1.17°	13.5	5.9 <sup>2</sup>	0	17
Vie	VIE	46.72° – 1.91°	0.55	4.4 <sup>2</sup>	100	16
Vilaine	VIL	47.49° – 2.46°	12.12	1.35 <sup>1</sup>	98	5

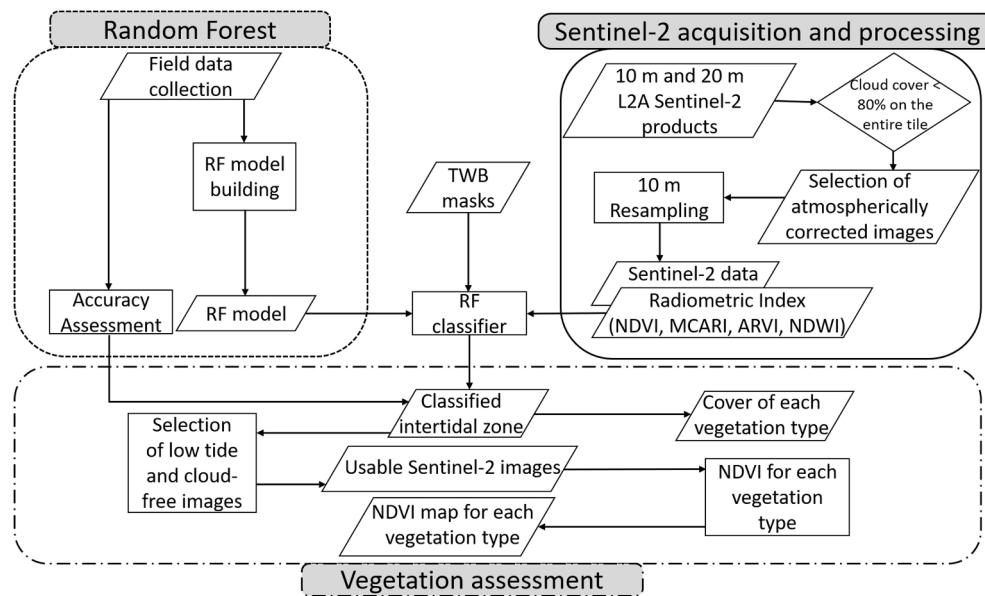


**Fig. 3.** Schematic representation of the workflow. L2A Sentinel-2 products are radiometrically and geometrically corrected. Sentinel-2 images are projected in UTM/WGS84 zone 30N or in UTM/WGS84 zone 31N, depending on the TWB latitude. Parallelograms symbolize input and output data. Rectangles indicate R scripts and rhombi are decisions taken by the user.

they did not improve the classification accuracy (Huete, 1988; Liu and Huete, 1995). Predictive variables were selected using Principal Component Analysis (PCA), which helped to reduce processing time (Zhang and Suganthan, 2014). The  $m_{try}$  parameter was set to 4, as  $m_{try} = \sqrt{p}$  (Belgiu and Drăgu, 2016), where  $p$  is the number of predictor variables; 14 in our case (ten S2 bands plus four multispectral indices).

### 2.5. RF classification accuracy assessment

The intertidal vegetation of the 26 French estuaries and bays was classified using the RF classifier described above. To assess the accuracy

of these classifications, an additional field campaign, synchronous with an S2 image acquisition, was conducted in June 2019. Vegetation present in the intertidal zone of Bourgneuf Bay was delineated to create a validation dataset of 66 polygons (Supplementary S3). The data consisted of the area (m<sup>2</sup>) and position (latitude-longitude) of each type of vegetation. A standard remote sensing error matrix was obtained (Congalton, 1991), and the kappa coefficient was calculated. Each cell of this matrix represents the number of classified pixels, where rows are the RF classified training data, and columns are validation data for the classification assessment. The intersection of rows and columns with the same name represents well-classified pixels. The overall accuracy of the

model is the ratio of well-classified pixels to the sum of all pixels. The Producer's accuracy of each class is the ratio of correctly classified pixels to the total number of validation data of the same class. Conversely, the User's accuracy is the number of correctly classified pixels in one class divided by the number of pixels classified in the same class. For each class identified by the RF classifier, the average NDVI and the class percent cover relative to the intertidal area was obtained. For the class MPB, an NDVI range of 0–0.37 was used. The upper threshold corresponds to the value proposed by (Méléder et al., 2003a,b) adapted for S2.

## 2.6. Image selection

In order to remove images with clouds over the intertidal zone, a cloud class was created during the RF model building process to detect clouds for each study site. All images with cloud cover greater than 10% over the intertidal zone were discarded. A second selection step was applied to the water level. The water level corresponding to the time of S2 acquisitions and the time of low tide were retrieved for each site from the website <http://maree.info/>. Low tide images were determined based on water height and the time difference between image acquisition and low tide ( $\pm 2$  h). Finally, 256 images were analyzed for the rest of this study, i.e. 28% of the initial total number, unevenly distributed between the sites (Table 1).

## 2.7. Environmental data

When available for all sites, environmental variables expected to have an effect on the microphytobenthos were extracted for each TWB from the Naiades database (<http://www.naiades.eaufrance.fr/>) of the French Biodiversity Agency and the Geological and Mining Research Bureau (BRGM). A set of physical variables (water temperature, pH, turbidity, oxygen, and day length) was retrieved, as well as nutrient data (concentrations of nitrate, ammonium, phosphate, and silicate). All data were measured in the water column. For each variable, the annual mean was calculated and averaged for the period 2015–2018. The two main types of intertidal sediment, mud and sand, expressed in percent cover for each intertidal area, were obtained from a report by the Algae Technology and Innovation Center (CEVA, <https://www.ceva-algues.com/>) (Le Bris et al., 2019).

## 2.8. Statistical analysis

First, ordinations based on remotely sensed intertidal vegetation variables (NDVI-MPB, NDVI-Green macroalgae, % cover MPB, % cover green macroalgae) were performed to analyze similarities between sites. For this analysis, the two main types of intertidal vegetation identified by the RF classifier were retained: microphytobenthos and green macroalgae. We used the metric Multidimensional Scaling approach (mMDS, Clarke and Warwick, 2001) with Euclidean distance to plot each site in a 2D space with a low projection distortion (stress of 0.05). Groups statistically significant at  $p < 0.05$  were identified through an analysis of similarity (ANOSIM). Bubble plots were used to highlight differences between groups of estuaries (Clarke and Warwick, 2001). This ordination analysis was performed using the PRIMER® software package. The groups of sites identified through mMDS were compared with Box and whisker plots. After checking normality with the Shapiro-Wilk test, a non-parametric Kruskal-Wallis followed by *a posteriori* Mann-Whitney pairwise comparisons were applied to test for statistically significant differences between groups. All univariate tests were performed using PAST 3.25 (Hammer et al., 2001). Relationships between environmental variables and remotely sensed data were first analyzed with univariate Spearman correlations (non-normality checked with Shapiro-Wilk). Finally, a multivariate analysis was performed using the two-table coupling method of Redundancy Analysis (RDA) (Legendre and Legendre, 1998), using the R package, *Vegan*. This

was used to elucidate MPB and green macroalgae patterns in relation to environmental variables and study sites. A Monte Carlo permutation test with 499 permutations was applied to test for statistical significance between environmental factors and their effects on intertidal vegetation. The analysis provided the significance of the eigenvalues and correlations to the canonical axes. All environmental data were normalized.

## 3. Results

### 3.1. Main characteristics of the study sites

The spatial distribution of French estuaries and bays analyzed in this study covers almost seven degrees of latitude, from the bay of Somme in the English Channel (50.22°N) to the Bidassoa estuary in the southern part of the Atlantic coast next to the Spanish border (43.37°N) (Fig. 1, Table 1). They are characterized by marked differences in their intertidal areas, with bays of tens of km<sup>2</sup> and narrow riverine estuaries, such as the Vie estuary with 0.55 km<sup>2</sup>. Furthermore, they are also characterized by different tidal ranges, from meso- to mega-tidal (Table 1). The highest ranges are found in bays of the English Channel (Mont Saint-Michel Bay, Bay of Veys, and Bay of the Somme), with up to 10 m of tidal range. The majority has a macro-tidal regime with a tidal range of between 4 and 7 m. An important consideration for MPB is the nature of the sediment, which is associated with different growth forms. The sites are characterized by contrasting sediment types: the majority is composed of muddy sediment, but there are some sandy estuaries and bays, notably those from the English Channel (Table 1).

### 3.2. RF classification and accuracy

The RF classification was performed for each site and each date available per site (Table 1). For 2018, five of the sites had three to five usable images for each site, and nine sites had more than ten usable images. A representative example of the RF classification is presented for the Penzé estuary in Brittany (Fig. 4). In this muddy-sandy estuary, the RGB true color composite S2 image from June 2018 showed that the downstream intertidal area was dominated by green macroalgae (Fig. 4A). Of the eight classes, the RF classifier identified green macroalgae as dominating the intertidal vegetation, with 44% cover, but also found that MPB occupied 21% of the intertidal zone, notably in the narrow, upstream section of the estuary (Fig. 4B). For the pixels classified as MPB, the NDVI was calculated as a proxy of MPB biomass (Fig. 4C). NDVI was similarly calculated for green macroalgae (not shown).

On average across all study sites, the two main benthic primary producers present at the surface of TWB tidal flats were MPB and green macroalgae, covering 10.2% (s.d. = 8.6%) and 5% (s.d. = 5.5%) respectively. In the English Channel, MPB covered only 2.3% of the intertidal areas (2.1% for green macroalgae) versus 15.1% for estuaries in Brittany (7.8% for green macroalgae) and 7.9% for the southern part of the Atlantic coast (2.7% for green macroalgae). The accuracy assessment of the RF classification is presented in Table 2. The error matrix indicated that overall map accuracy was 91%, with a kappa coefficient of 0.84. MPB showed a Producer's accuracy of 84% and a User's accuracy of 94%. The lower Producer's accuracy indicates that the RF did not detect all MBP seen in the field, with some pixels being classified as bare mud. This suggests an underestimation of MPB presence. It appears that MPB biomass with an NDVI of less than 0.12 (*ca.* 1 mg chlorophyll *a*.m<sup>-2</sup> estimated from Méléder et al., 2003b) cannot be detected by the Random Forest. For green macroalgae, the Producer's accuracy was 88% and the User's accuracy was 59%. The lower green macroalgae User's accuracy was mainly due to confusion with marine angiosperms (slikke and schorre angiosperm).

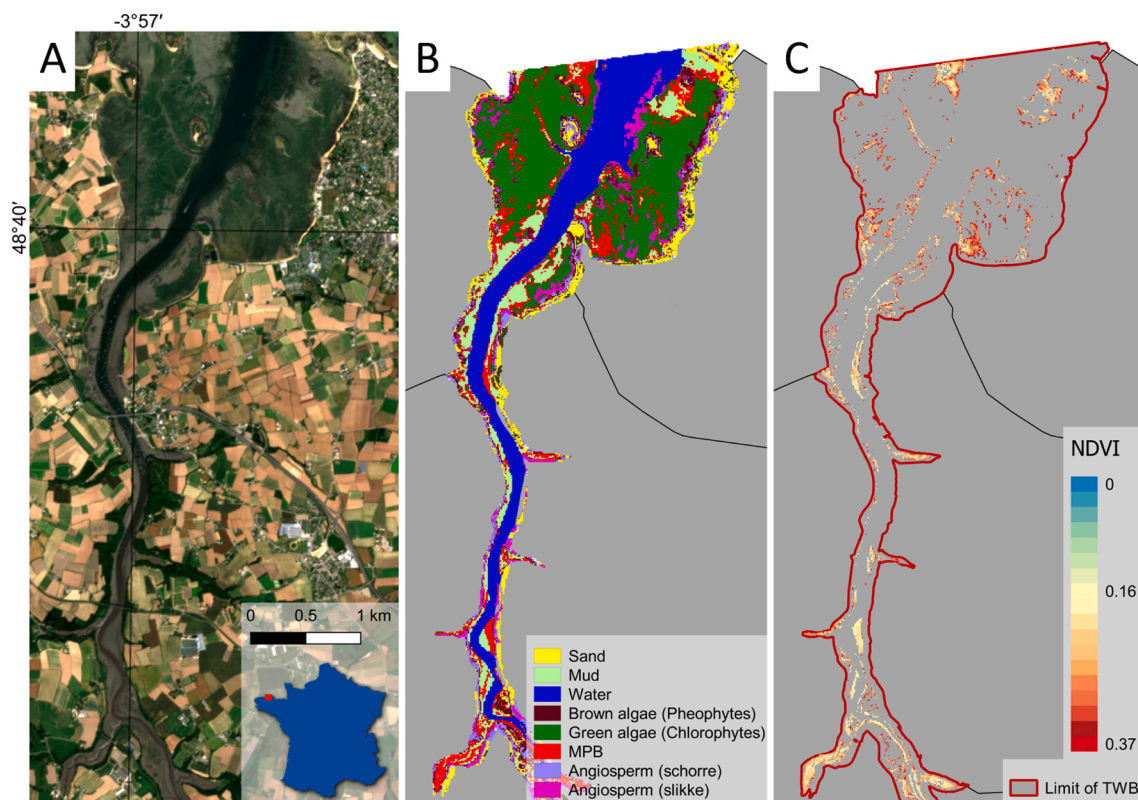


**Fig. 4.** Sentinel-2 RGB composite (A), Random Forest classification (B), and NDVI for the microphytobenthos (MPB) class (C) for the Penzé estuary. The schorre is the upper vegetated intertidal zone; the slikke is the lower intertidal zone occupied by mudflats. The boundaries of the estuary correspond to the Transition Water Body (TWB) perimeter defined by the French Agency of Biodiversity.

**Table 2**

Confusion matrix of the Random Forest (RF) model. Columns are classes seen in the field and rows are the results of RF classification. The intersection between columns and rows are well-classified pixels. The intersection between Producer's and User's accuracy is the overall accuracy of the RF model. "Angiosperm refers to both slikke and schorre angiosperm.

	Sand	Bare mud	Brown macroalgae	Green macroalgae	Angiosperms	MPB	User's accuracy
Sand	500	6	24	0	0	3	0.94
Bare mud	54	5735	1	4	0	233	0.95
Brown macroalgae	1	0	567	9	23	0	0.95
Green macroalgae	0	0	4	775	441	96	0.59
Angiosperms	0	0	43	36	1082	0	0.93
MPB	19	29	7	57	0	1759	0.94
Producer's accuracy	0.87	0.99	0.88	0.88	0.70	0.84	0.91

### 3.3. Ordination of the TWBs

Annual median NDVI and percent cover for both MPB and green macroalgae were calculated for each TWB (Fig. 5). There was a stronger gradient between estuaries in percent cover compared to NDVI. The Aulne estuary (AUL) had the greatest intertidal surface MPB cover (26%), while Mont-Saint-Michel Bay (MON) had the least (0.5%) (Fig. 5A). Green macroalgae percent cover was greatest in the Auray estuary (AUR; 13.6%) and lowest in the Sèvre Niortaise estuary (NIO; 0.3%). Some estuaries, such as the Penzé (PEZ), showed high percent cover of both MPB and green macroalgae. Overall, there were significant differences in median percent cover of both MPB and green macroalgae between estuaries (Kruskal-Wallis,  $p < 0.05$ ). The estuaries differing from each other were identified with the following ordination. Median NDVI for MPB ranged between 0.23 (NIO) and 0.28 (AUR), while green algae NDVI showed higher values, ranging from 0.42 (Vilaine, VIL) to 0.51 (Trieux, TRI). There were significant differences in the median NDVI of both MPB and green macroalgae between estuaries (Kruskal-

Wallis,  $p < 0.05$ ).

Using NDVI and percent cover of both MPB and green macroalgae, the 26 study sites were represented using a metric multidimensional scaling (mMDS) analysis, comparing their similarities based on Euclidian distances (Fig. 6). The mMDS showed that the TWBs were grouped in three significant clusters (Fig. 6A, ANOSIM;  $p < 0.05$ ). These group could only be partially explained by geography: all sites of the English Channel were in group 1, mixed with estuaries from Brittany and the southern part of the Atlantic coast, which also constituted group 2. Group 3 was only composed of estuaries from Brittany. The ordination showed a marked gradient of colonization of the intertidal zone by the main benthic primary producers (Fig. 6B), ranging from low (group 1) to high (group 3). Group 3 had the highest percent cover of both MPB and green macroalgae. Estuaries with the greatest MPB coverage were estuaries where the percent cover of green macroalgae was also higher. Conversely, estuaries with a low percent cover for one vegetation type also had low coverage of the other type. The Trieux estuary had a unique composition, characterized by a low percent cover of MPB but a high

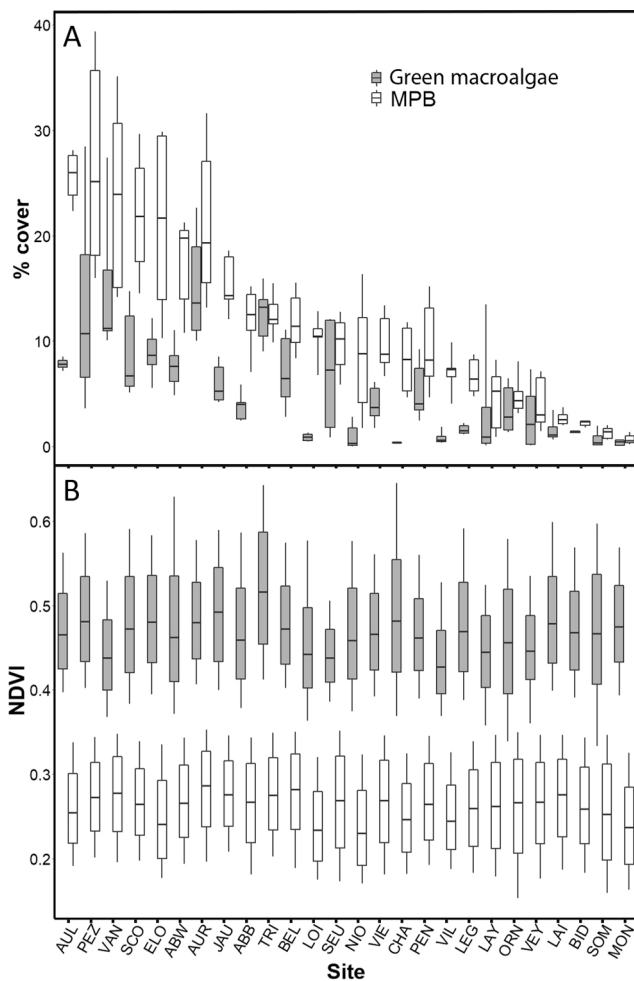


**Fig. 5.** Box and whisker plots of both green macroalgae and microphytobenthos (MPB) median percent cover (A) and NDVI (B) for the 26 French estuaries and bays presented in Fig. 1. Boxes represent quartiles Q1 (25%), Q3 (75%), and the median. Whiskers represent Q10 (10%) and Q90 (90%). Abbreviations are detailed Table 1.

percent cover of green macroalgae. The type of intertidal sediment appeared to be relevant to the interpretation of the ordination, in particular for MPB, with group 1 mainly composed of sandy bays and estuaries, and group 3 associated essentially with muddy sediment (Fig. 6C). However, within each group, the idiosyncratic response of some estuaries to sediment type suggested that other variables needed to be considered. There was a significant difference in the median NDVI of MPB between the three groups (Kruskal-Wallis,  $P < 0.01$ ), with group 1 significantly lower (*a posteriori* Mann-Whitney pairwise,  $P < 0.01$ ) (Fig. 7A). Differences were significant between all groups for MPB percent cover (Kruskal-Wallis,  $P < 0.01$  and *a posteriori* Mann-Whitney pairwise,  $P < 0.01$ ), with a marked gradient likely contributing to the ordination (Fig. 7B). The median MPB percent cover for group 1 was less than five but was more than 20 for group 3. A similar analysis was done for macroalgae, with significant differences between all groups for percent cover (Kruskal-Wallis,  $P < 0.01$  and *a posteriori* Mann-Whitney pairwise,  $P < 0.01$ ) (Fig. 7C, D). The median macroalgae percent cover of was less than 2% for group 1 but more than 8% for group 3. The first group comprised sandy estuaries, and was significantly different from the two others, which were strictly composed of muddy sediment (Fig. 7E) (Kruskal-Wallis,  $P < 0.01$  and *a posteriori* Mann-Whitney pairwise,  $P < 0.01$ ). The sandy estuaries were characterized by a significantly lower concentration of phosphates in the water column (Fig. 7F) (Kruskal-Wallis,  $P < 0.01$  and *a posteriori* Mann-Whitney

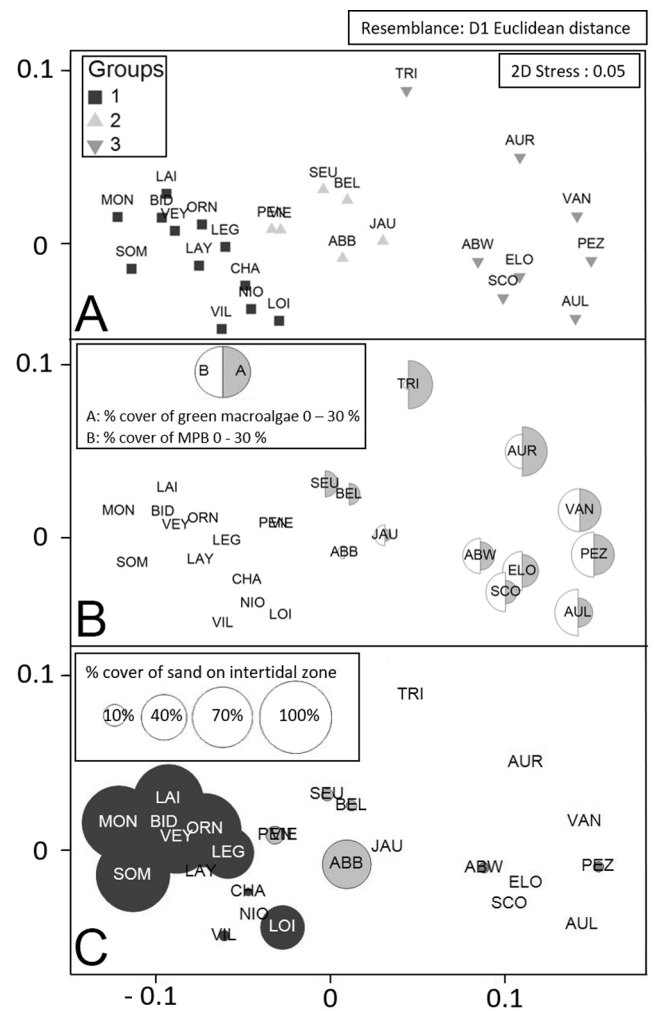


**Fig. 6.** Ordination of the 26 French estuaries and bays presented in Fig. 1 using metric Multi-Dimensional Scaling (mMDS) based on NDVI and percent cover of microphytobenthos (MPB) and green macroalgae. Estuaries and bays were grouped in three significant clusters (ANOSIM,  $p < 0.01$ ) (A). Contribution of the percent cover of MPB and green macroalgae to the ordination (B). The size of bubbles are proportional to the percent cover of each vegetation type. The maximum % cover for the two types of vegetation is 30%. The largest bubbles correspond to 30%. Percent of the intertidal zone covered by sandy sediment (C). Abbreviations are detailed in Table 1.

pairwise,  $P < 0.01$ ). Group 3, with the highest MPB and macroalgae percent cover, also had a significantly higher concentration of silicates in the water column (Fig. 7F) (Kruskal-Wallis,  $P < 0.01$  and *a posteriori* Mann-Whitney pairwise,  $P < 0.01$ ). No statistical difference was found between the groups in terms of nitrate concentration (Kruskal-Wallis,  $P = 0.31$ ), but group 1 was characterized by a lower median concentration ( $19.46 \text{ mg.L}^{-1} = 313 \text{ } \mu\text{mol.L}^{-1}$ ) than groups 2 ( $25.04 \text{ mg.L}^{-1} = 404 \text{ } \mu\text{mol.L}^{-1}$ ) and 3 ( $21.32 \text{ mg.L}^{-1} = 344 \text{ } \mu\text{mol.L}^{-1}$ ). For all sites, nitrates represented more than 95% of the nitrogen forms.

#### 3.4. Relationship between MPB and environmental variables

A preliminary univariate correlation analysis showed that MPB NDVI correlated positively with silicate ( $r_s = 0.58$ ,  $p < 0.001$ ), for and somewhat with phosphate ( $r_s = 0.38$ ,  $p = 0.05$ ), but correlated negatively with temperature, turbidity, and pH ( $r_s = -0.48$ ,  $r_s = -0.52$ , and  $r_s = -0.57$  respectively, all with  $p < 0.001$ ). MPB percent cover correlated positively with mud ( $r_s = 0.69$ ,  $p < 0.001$ ) and negatively with sand and pH ( $r_s = -0.64$ ,  $p < 0.001$  and  $r_s = -0.56$ ,  $p < 0.01$

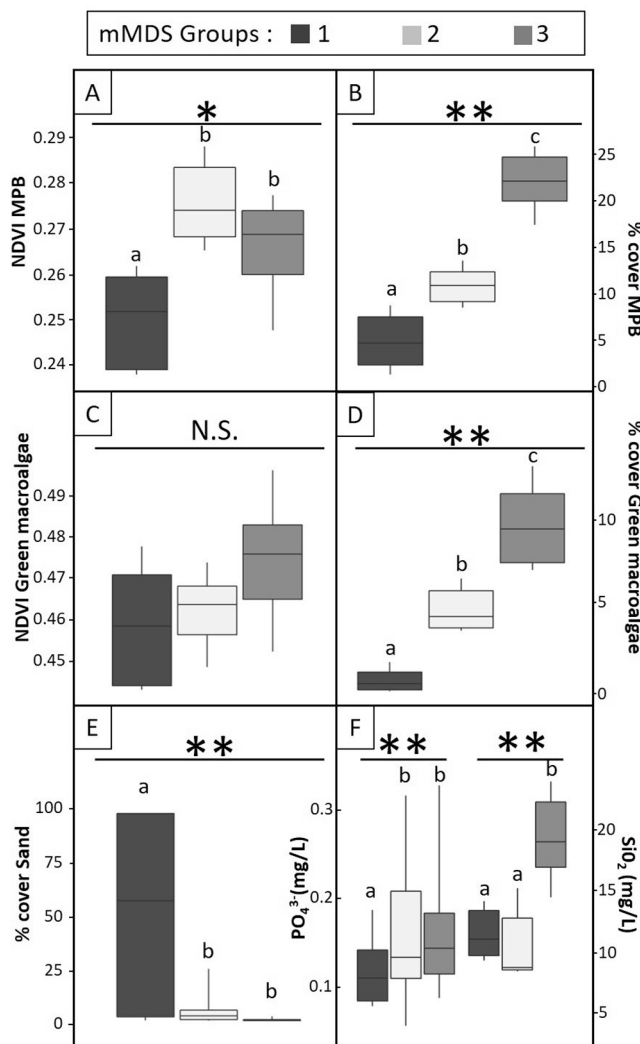


**Fig. 7.** Box and whisker plots of variables associated with the three groups of estuaries and bays identified in Fig. 6 using mMDS ordination. Microphytobenthos (MPB) NDVI (A) and percent cover (B); green macroalgae NDVI (C) and percent cover (D); percentage of the intertidal zone covered by sandy sediment (E); and concentrations of orthophosphates and silicates in the water column (F). Boxes represent quartiles Q1 (25%), Q3 (75%), and the median. Whiskers represent Q10 (10%) and Q90 (90%). Asterisks indicate statistically significant differences (\*\*:  $p < 0.01$ ; \*:  $p < 0.05$ , n.s. = not significant) between groups that do not share the same letter.

respectively). NDVI and green macroalgae percent cover correlated negatively with pH ( $r_s = -0.43$  and  $r_s = -0.59$  respectively, both with  $p < 0.05$ ). The green macroalgae percent cover also correlated negatively with turbidity ( $r_s = -0.50$ ,  $p < 0.01$ ). There was a strong positive correlation between the percent covers of MPB and green macroalgae ( $r_s = 0.77$ ,  $p < 0.001$ ). A redundancy analysis (RDA) was performed to analyze the ordination between MPB and green macroalgae, environmental variables, and the study sites (Fig. 8). The RDA accounted for 59.8% of the total variance (all canonical axis). Of this, 98% was explained by the two first axes. These two canonical axes were significant ( $p < 0.05$ ). Concerning variables, water temperature, sediment, and turbidity were significant ( $p < 0.05$ ), while all others were not ( $p > 0.05$ ). The first axis mainly opposes mud and nutrients to the other abiotic variables. The second axis opposes silicates to turbidity. This RDA shows that the percent cover of green algae is related to nutrients (nitrate, phosphate, and silicate) and oxygen. MPB percent cover is linked to the presence of mud, but also to nutrients. The NDVI of MPB and green macroalgae are more related to water temperature, pH,

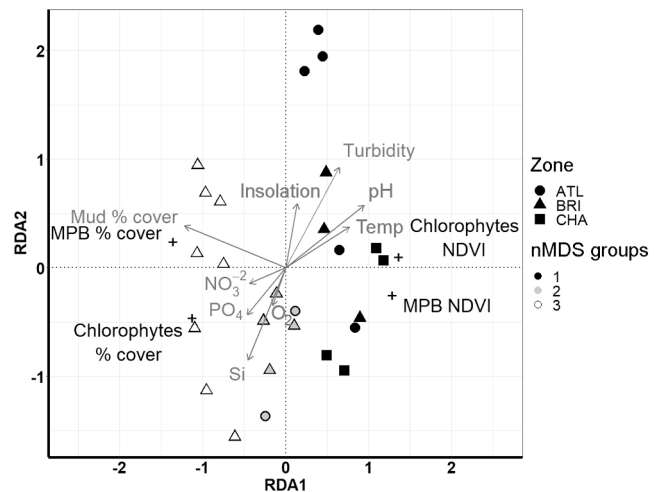


**Fig. 8.** Redundancy Analysis (RDA) plot with sites (symbols), environmental variables (vectors and grey texts), and remotely-sensed variables (bold text). Sites are divided into three groups by geographical position: mid-French Atlantic coast (ATL); Brittany (BRI), and eastern English Channel (CHA). nMDS groups were created using Euclidean distances (cf Section 3.3).

turbidity, and insolation. The RDA is coherent with the nMDS ordination. The nMDS group 3, which is exclusively composed of muddy estuaries, is related to mud percent cover and is opposed to group 1, which includes all sandy estuaries. Geographic patterns are less discernable. Sandy estuaries of the eastern English Channel are clustered together. All other estuaries are mixed and distributed along the RDA axis 2, however, the majority of Brittany estuaries are associated with nutrients.

## 4. Discussion

### 4.1. Identification of MPB with a Random Forest classifier

In this study, we identified MPB-colonizing estuaries and bays with a Random Forest (RF) algorithm (Breiman, 2001), a machine learning classifier that has only recently been applied to map tidal flats, as well as intertidal and subtidal vegetation (Fairley et al., 2018; Martin, 2020; Murray et al., 2019; Traganos and Reinartz, 2018a,b; Wang et al., 2018). However, to our knowledge, it has not yet been used to map intertidal vegetation composed of photosynthetic unicellular organisms and has mainly been applied to identify vascular plants. MPB is characterized by a significantly lower NIR reflectance compared to macroalgae and marine angiosperms (Méléder et al., 2003b), and therefore has a more discrete spectral fingerprint. Very often, diatoms are the dominant component of MBP (MacIntyre et al., 1996), with characteristic spectral features including the chlorophyll-*c* absorption band at 632 nm and a spectral shape at around 550 nm due to the presence of fucoxanthin (Méléder et al., 2003b). However, at the spectral resolution of S2, it was not possible to use these spectral features and to apply dedicated spectral indices (Launeau et al., 2018). The main methodological challenge was therefore to discriminate MPB from intertidal macrophytes with limited spectral information. This spectral constraint was overcome by the RF classifier that was built using 14 predictor variables, ten S2 bands in the VIS, NIR, and SWIR, and four vegetation indices, NDVI, NDWI, ARVI, and MCARI. Other vegetation indices were tested, but were not retained, as they did not improve the classification accuracy, but increased computational time.

The RF classification was developed to discriminate each type of intertidal vegetation, but was also used in the preliminary stage of image selection, based on cloud coverage and water height. Thick, opaque clouds, such as cumulus, were efficiently detected, but thin, transparent

clouds, such as cirrus, were more problematic. To avoid selecting images with this type of cloud over intertidal areas, we applied conservative thresholds, which probably reduced the number of images retained that could have been exploited. In total, 918 Sentinel-2 images were downloaded and classified for 2018. It took *ca.* 200 h using the Caret R package on a standard PC to process. *Ranger* is a new package developed for R, implementing a C++ version of the RF algorithm (Wright and Ziegler, 2017), providing a faster runtime and more efficient memory usage. The number of trees used to create the RF model was set to 500 after testing different numbers (100, 250, 500, 1000, and 2000), as the same accuracy was obtained compared to higher values while limiting processing time (Thanh Noi and Kappas, 2017). In fact, RF accuracy is more sensitive to the  $m_{try}$  parameter, which sets the number of predictive variables to be selected and tested when growing the trees (Kulkarni and Sinha, 2012). Increasing  $m_{try}$  can improve the accuracy of the final model, but it greatly increases the processing time, so we kept a value of 4 (Ghosh et al., 2014).

The accuracy of the RF classifier was estimated using field data collected from three distinct sites. Overall, high accuracy was achieved for the identification of MPB, in terms of both User's and Producer's accuracies, which were 94% and 84% respectively. The lower Producer's accuracy was due to confusion with bare mud, which suggests that the classifier did not detect the lowest MBP biomass. In fact, 13% of the MPB delineated in the field with a hand-held GPS was classified as bare mud by the RF. The classifier therefore slightly underestimated the detection of MPB, but when it was detected, the MPB maps were very accurate. Conversely, bare mud and sand observed in the field were correctly classified as such with high accuracy, which means that bare substrates were not mistaken for MPB. The question of where to set a detection threshold for bare backgrounds to avoid confusion with MPB is not trivial (Launeau et al., 2018). Bare mud or bare sand reflectance spectra are characterized by positive slopes between their red and NIR reflectance and therefore display non-null values for NDVI-like indices (Barillé et al., 2011). Setting empirical NDVI thresholds has been proposed to avoid overestimating MPB where bare sediment is present (Launeau et al., 2018).

The green macroalgae seen in the field during the validation campaign was correctly detected (Producer's accuracy of 88%), but the RF classifier also included angiosperms in this class, leading to a lower User's accuracy of 59%. The confusion between these two macrophytes was probably related to their similar pigmentary composition, in particular with respect to chlorophyll-*b*. To improve the mapping of these two intertidal macrophytes, an idea would be to test an additional set of texture layers as predictor variables in the machine learning classifier (Martin, 2020). Object-based image analysis has the potential to improve classification performance (Poursanidis et al., 2018), as has been shown for seagrass (Duffy et al., 2018; Roelfsema et al., 2014). Among the latest state-of-the-art methods, extreme gradient boosting (Xgboost) has been described as outperforming other machine-learning methods for very high-resolution remote sensing data (Georganos et al., 2018a,b). However, this method needs a huge training dataset and corresponds to long computation times (Georganos et al., 2018b). LightGBM is another promising approach to classify objects using optical remotely-sensed data (Zhong et al., 2020), but was not compared to RF.

The RF model accuracy could be improved by increasing the training and validation dataset across a higher number of sites, notably sandy estuaries. The size of the training data is related to the overall accuracy of the model (Du et al., 2015), and training data from each class should represent at least 0.25% of the studied area (Colditz, 2015; Thanh Noi and Kappas, 2017). In our case, this rule was respected for all classes, except for brown algae. The RF was identified as the most stable machine learning algorithm in terms of overall accuracy when the model is trained on multiple study sites, as we did (Vettrivel et al., 2015). The current RF algorithm can certainly be fine-tuned, but the present study already demonstrates that an off-the-shelf methodology (RF is available in commercial software such as ENVI©, or on the Sentinel Application

Platform (SNAP) from the European Space Agency) can quantitatively assess the spatial distribution of MPB in estuaries using S2 images. Along with the fact that these images are provided atmospherically corrected via the Copernicus platform, this increases the interest of developing such a bioindicator for transitional waters as it reduces the processing complexity. This study validated the hypothesis that S2 spectral resolution is suited to intertidal vegetation discrimination.

#### 4.2. Sentinel-2 spatial and temporal resolutions for intertidal microphytobenthos

One of our hypotheses was that the S2 spatial resolution is adapted to map small estuaries, in particular those with a riverine morphology. These estuaries have narrow intertidal zones parallel to the riverbed. In this study, all estuaries were able to be observed with a 10 m spatial resolution, even the Vie estuary, which has an intertidal surface of 0.55 km<sup>2</sup> (Table 1). When testing for even smaller estuaries (not considered in this study), such as the Nivelle estuary (43°22'52" N, 1°39'30" W), which has an intertidal surface of 0.13 km<sup>2</sup> (*ca.* one thousand 10 m pixels), it was possible to run the RF and retrieve information. In fact, only the right bank of this estuary, which has very narrow tidal flats parallel to the river and represents less than three pixels, could not be observed. In addition to the 26 TWBs of this study, we verified that all French TWBs (43 in total) are mappable with S2. These findings are consistent with the results of Schaeffer and Myer (2020), who indicated that a spatial resolution of at least 15 m was necessary to map long and narrow riverine estuaries in the continental United States. NASA's Landsat series spans more than 30 years and the Operational Land Imager (OLI) sensor of Landsat 8 is comparable to S2 MSI, but the spatial resolution in multispectral mode is 30 m (Barsi et al., 2014). Landsat was successfully used to map the worldwide distribution of tidal flats (Murray et al., 2019), but not all French estuaries can be observed at this resolution (Ribeiro et al., 2018).

Sentinel-2 is a constellation, acquiring images between 11 and 12 UTC at our study sites, with a minimum revisit time interval of five days (Bergsma and Almar, 2020). At European latitudes, the expected median cloud coverage is approximately 50% (Bergsma and Almar, 2020), and the high S2 revisit time compensates for missing observations due to cloud cover. This offers a good probability of obtaining coastal parameters for shallow water studies (Kutser et al., 2020), but there is an additional strong tidal constraint for the observation of intertidal zones. In this study, where all S2 images available for the year 2018 were downloaded, only 28% were exploitable due to the combined constraints of cloudiness and low tide. The frequency of images was unevenly distributed between estuaries, with three being under sampled (less than five images acquired per year), while ten had more than ten images per year. However, when analyzed by season, the frequency distribution was comparable between the three regions considered, with fewer images available in winter (Supplementary S1). This was not systematically related to the size of the estuary, although open bays were more frequently observed.

These numbers must, however, be put into perspective with previous studies on intertidal MPB. Time-series analysis of SPOT images used only one image per year (Benyoucef et al., 2014; Echappé et al., 2018; Méléder et al., 2003b), while MPB seasonal variation was assessed with five images in the Tagus estuary (Brito et al., 2013). A much higher temporal resolution was achieved using the Moderate Resolution Imaging Spectroradiometer (MODIS) (Savelli et al., 2018; van der Wal et al., 2010), but with 250 m pixels. However, only the largest French estuaries can be resolved at this spatial resolution (Ribeiro et al., 2018). Sentinel-2 therefore significantly improved the probability of high-resolution multispectral observations of intertidal MPB. The time of acquisition, between 11 and 12 UTC, is well-adapted to all estuaries of the Atlantic coast and Brittany, because it coincides with low tide on the days of spring tides. This is when the largest tidal range occurs, with maximal exposure of the tidal zone around midday, which corresponds

to favorable conditions for photosynthetic organisms. However, this is not the case in the eastern English Channel, where low water levels of spring tides occur early in the morning or at the end of the day (Spilmont et al., 2006). This creates a discrepancy from the Seine estuary to the sites located at the Belgian border. For these estuaries, Sentinel-2 only captures neap tides, when less intertidal surface is exposed compared to low spring tides. One challenge is that, even with two orbital cycles, only one tidal phase can be observed in both the Atlantic (spring tides) or the eastern English Channel (neap tides) (Supplementary S2). The consequences of mapping MPB at different phases of the fortnightly cycle remains to be investigated.

#### 4.3. MPB relationship with environmental variables

Several abiotic (e.g., temperature, salinity, nutrients, light, pollutants, wind and waves, tidal elevation, sediment type) and biotic (grazing, interspecific competition) factors can explain the spatio-temporal distribution of estuarine MPB (Admiraal, 1984; Savelli et al., 2018), but causal relationships are always difficult to establish with statistical relationships obtained using *in situ* data (Brotas et al., 1995). The high variability of estuarine sediment physico-chemical conditions across seasonal, fortnightly, and semi-diurnal tidal cycles, and the interplay between variables contributes to this complexity. However, the influence of environmental factors on MPB biomass and distribution generally depends on the spatial scale of observation (Murphy et al., 2008; Saburova et al., 1995). At the whole ecosystem macroscale (kilometric) of remote sensing observations, abiotic variables are expected to explain the main patterns (Daggers et al., 2020), while biotic variables tend to be related to MPB patchiness at the microscale (centimetric) (Weerman et al., 2011).

In this study, both univariate and multivariate analysis has shown that sediment type was one of the main factors responsible for the differences between estuaries. This result is consistent with previous studies (Brotas et al., 1995; Oh and Koh, 1995; Orvain et al., 2012) that showed that the spatial distribution of benthic microalgae at the macroscale was mainly related to the granulometric composition of sediments (Méléder et al., 2005; Paterson and Hagerthey, 2001), emphasizing that sediment type integrated other variables, such as sediment stability, deposition of organic particles, and interstitial water quality. In soft-bottom assemblages, MPB is divided into epipsammic species common in sandflats, where cells are attached to or almost immobile on sand grains, and free-living epipellic species that usually dominate mudflats (Admiraal, 1984). Muddy sediments colonized by epipellic growth-forms are characterized by higher MPB biomass favored by an accumulation of nutrients and the stability of sediment (Méléder et al., 2005; Paterson and Hagerthey, 2001). The higher NDVI found in this study for the muddy sites is consistent with previous observations of MBP spatio-temporal distribution in estuaries from northern Europe (van der Wal et al., 2010). Remote sensing data can only retrieve the sediment surface present in the photic layer: ca. 500  $\mu\text{m}$  max for mud and ca. 2 mm for sand (Paterson and Hagerthey, 2001). The deeper sediment cannot be seen by the sensor, and the NDVI of sandflats corresponds at most to a ca. 2 mm depth. However, even integrated over such a depth, the biomass of epipsammic species remains lower than the biomass of epipellic species colonizing the first 500  $\mu\text{m}$  of muddy sediment (Cartaxana et al., 2011; Morelle et al., 2020). Sediment type was therefore a strong structuring factor when comparing the 26 sites through multivariate analysis, and the estuaries with the largest surface covered by MPB were always associated with muddy sediment. However, not all muddy sites had a high MPB percent cover, which suggests that other variables should explain the MPB distribution in French estuaries.

Interestingly, MPB percent cover was significantly correlated with green macroalgae percent cover. In this study, the estuaries characterized by the greatest green macroalgal coverage were located in Brittany. In this region, estuaries and coastal areas are known for the development

of opportunistic green macroalgae in response to coastal eutrophication (Perrot et al., 2014). Brittany has the highest nitrate concentrations in estuaries due to intensive farming activities (Ménèsquen et al., 2018). Even though significant statistical relationships were not detected, the trend observed in the RDA analysis suggests that estuaries covered by green macroalgae are, indeed, those with high nutrients concentrations. Airborne campaigns performed in 2018 on four muddy sites (TRI, VAN, PEZ, ABW), confirmed S2 observations of green macroalgae coverage (Ballu, 2019). For MPB, univariate correlations showed that NDVI was significantly related to silicate and to a lesser degree to phosphate concentrations. There was a significant correlation between phosphate and silicates for muddy sites ( $R_s = 0.58$ ,  $P < 0.01$ ) suggesting a possible sedimentary origin of these nutrients rather than fluvial inputs. In fact, phosphorus is adsorbed on seston and accumulates in the sediment (Ratmaya et al., 2018; Riaux-Gobin, 1985).

These two nutrients were also significantly related to MPB assemblages on coastal mudflats of the French Atlantic coast (Du et al., 2017). However, the redundancy analysis did not confirm this relationship between NDVI and nutrients. In fact, there was much less variation in MPB NDVI compared to MPB percent cover (Fig. 5). In sandy estuaries, the MPB percent cover can be less than 3% of the whole estuary, but a high NDVI value can be obtained from a few pixels identified as MPB by the Random Forest. We therefore suggest that in the methodological framework of this study, MPB percent cover is more suitable than MPB NDVI as a bioindicator.

We are aware that this analysis is limited, firstly because there were no nutrient data for the sediment (this is also true for all parameters), secondly, because the analysis was based on annual medians, whereas nutrients and other variables have a seasonal cycle, and thirdly because correlations may not be causal. This is probably the case of the negative correlation between MPB NDVI and temperature: in this study, the highest MPB biomass was observed in Brittany estuaries characterized by an annual median temperature 1 or 2 °C lower than the other sites. On the other hand, the positive correlation between MPB NDVI and silicates may be causal as benthic diatom growth can be limited by the supply of silicates for their silica frustule. Similarly, the negative correlation between MPB and pH may be explained by a higher inorganic carbon depletion at high pH, a key component of photosynthesis (Vieira et al., 2016). Despite the limitations of this macroscale and annual approach, we observed consistent trends that merit further investigation, and the following subsection proposes suggestions for improvement.

#### 4.4. Developing a MPB bioindicator for estuaries using Earth observation data

Benthic microalgae have long been used in rivers and streams to assess environmental conditions (Stevenson et al., 2010). Phytoenthos is one the Biological Quality Elements used by the WFD as a bioindicator of river and lake quality (Kelly, 2013). This does not exist for transitional waters, and Trobajo and Sullivan (2010) stressed the need to develop water quality indices based on benthic microalgal assemblages in estuaries and shallow water environments. This is not specific to Europe; the review of MPB research in Korean tidal flats by Park et al. (2014) does not mention bioindication as a relevant topic. One of the challenges of estuaries is the high variability of abiotic variables, which generates natural stressors, making it difficult to detect anthropogenic effects, the so-called “estuarine quality paradox” (Elliott and Quintino, 2007). In such dynamic environments, traditional sampling methods lead to another uncertainty related to the location and number of sampling sites, and the number of replicates (Kelly, 2013; Stevenson et al., 2010). Moreover, MPB is characterized by significant spatial variability at the microscale (Spilmont et al., 2011). Satellite observations with their inherently large spatial coverage can overcome these problems and provide metrics estimated at the macroscale.

In this work, we retrieved two structural variables describing MPB

assemblages that were spatially integrated over the full water bodies. The first is the NDVI, a proxy of MPB biomass, which could potentially be an indicator of stress conditions, such as nutrients or sediment toxicity. The second is the MPB percent cover, which may respond to the same variables, but is more sensitive to hydromorphological changes at a larger, landscape scale. One consequence of studying MPB at a large spatial scale is the scale-dependence of environmental factors where higher-level factors (e.g., climate, geology) can be more constraining than lower-level ones, such as nutrients or pollutants (Stevenson, 1997). In this study, one of the main factors explaining the pattern of variation of MBP between the 26 French estuaries was sediment type. This can be regarded as a higher-level factor, which has partially masked the effect of lower-level factors, as suggested by the lack of statistical significance of nutrients in the redundancy analysis. This means that a single bio-indicator cannot be applied indiscriminately to all estuaries, which must instead first be considered by sediment type (e.g., sandy or muddy). The division between the two sediment types remains to be established, knowing that natural intertidal sediment generally consists of a mixture of sediment types (Paterson and Hagerthey, 2001).

A similar recommendation to standardize the sampling substrate has been proposed for freshwater benthic microalgae (Stevenson et al., 2010). These authors also proposed that first subdividing large data sets may reduce covariation among environmental factors and help the development of more causally-related indicators. We expect all environmental/anthropogenic data to become available for the 43 French TWBs, as a national database is currently being organized by the French Biodiversity Agency, and additional S2 data could be obtained to perform an analysis of sedimentary type of each estuary. A more ambitious outlook would be to expand this approach to other European estuaries identified as TWBs by the WFD.

Despite the almost thousand S2 images processed for a single year, it was not possible to get a clear picture of the MPB seasonal cycle for each estuary. A pattern of maximum biomass peaking in early spring, followed by a summer depression was observed for the Loire and Sèvre-Niortaise sites using MODIS (Oiry S. pers. comm.), but no information is available for the remaining sites. MPB seasonal variations observed in Dutch and United Kingdom estuaries and coastal sites using MODIS (van der Wal et al., 2010) were synchronized in disjointed ecosystems. An improvement of the method would be to estimate the MPB percent cover at peak biomass, but summer measurements could also be meaningful. In temperate areas, MPB biomass is generally low in the summer due to nutrient depletion at this time, grazing by herbivores, and thermo- and photoinhibition (Savelli et al., 2018). Higher biomass compared to a reference condition could be related to an abnormal input of nutrients or to lower grazing pressure due to an anthropogenic impact on grazers.

## 5. Conclusion

The 10 m spatial resolution of S2 enables the observation of all French TWBs for the WFD. With a machine learning classifier, it was possible to discriminate MPB from intertidal macrophytes (macroalgae and angiosperms) despite the multispectral resolution. S2 can, therefore, provide spatial metrics on MPB as a group of unicellular photosynthetic organisms at the macroscale. S2 image data is publicly available through ESA's sci-hub and EU Copernicus portals, and is therefore a good compromise to map estuarine microphytobenthos at no cost. This improved spatial and temporal coverage is a strong argument for the use of satellite data in complement to conventional sampling for the WFD statutory monitoring and reporting (Papathanasopoulou et al., 2019). This work is a first step toward a possible satellite water quality metric using MPB percent cover, as a bioindicator of high nutrients loads. This can be particularly useful in turbid estuaries where none of the biological water quality metrics based on phytoplankton or macroalgae can be applicable. This is the case for the three largest French estuaries: the Gironde, the Loire, and the Seine. Four recommendations can be made to improve the analysis: 1) to consider sandy and muddy estuaries

separately, 2) to extract the spatial information for the poly-haline and mesohaline sectors of estuaries, which can have different MPB biomass (Benyoucef et al., 2014), 3) to retrieve MPB structural variables from the mid-intertidal zone to the upper shore to account for the effect of tidal elevation on MPB spatial distribution (Brotas et al., 1995; van der Wal et al., 2010) and 4) to target specific periods of the MPB seasonal cycle.

## Author contributions

SO and LB conceptualized this study. SO performed data curation. SO and LB have done the formal analysis of the data. All authors wrote, reviewed, critically revised, and approved the final version of the manuscript.

## CRedit authorship contribution statement

**Simon Oiry:** Conceptualization, Data curation, Formal analysis, Methodology, Writing - original draft, Writing - review & editing. **Laurent Barillé:** Conceptualization, Formal analysis, Methodology, Writing - original draft, Writing - review & editing.

## Declaration of Competing Interest

The authors declare that they have no known competing financial interests or personal relationships that could have appeared to influence the work reported in this paper.

## Acknowledgments

This study was supported by a grant from the Office Français de la Biodiversité (OFB), France, grant number: 180906 – Convention Microphytobenthos Phase II. The European Space Agency is acknowledged for the provision of Sentinel-2 images. This study also benefited from CoastObs, a European Union Horizon 2020 research and innovation program (grant agreement number: 776348). The authors are much obliged to Philippe Rosa for his assistance during fieldwork and Bruno Jesus who helped with R codes for selecting images at low tide. We would like to thank Stephanie Palmer for her comments on the manuscript and for revising the English.

## Appendix A. Supplementary data

Supplementary data to this article can be found online at <https://doi.org/10.1016/j.ecolind.2020.107184>.

## References

- Admiraal, W., 1984. The ecology of estuarine sediment-inhabiting diatoms. In: Chapman, D.J., Round, F.E. (Eds.), *Progress in Phycological Research*. Biopress, pp. 269–322.
- Bailu, S., 2019. Suivi des blooms de macroalgues opportunistes sur le littoral Loire-Bretagne, Contrôle de Surveillance (RCS): Inventaires et qualification des masses d'eau. CEVA. Année 2018 81 pp.
- Barbier, E., Hacker, S., Kennedy, C., Koch, E., Stier, A., Silliman, B., 2011. The value of estuarine and coastal ecosystem services. *Ecol. Monogr.* 81 (2), 169–193.
- Barillé, L., Mouget, J.-L., Méléder, V., Rosa, P., Jesus, B., 2011. Spectral response of benthic diatoms with different sediment backgrounds. *Remote Sens. Environ.* 115 <https://doi.org/10.1016/j.rse.2010.12.008>.
- Barillé, L., Robin, M., Harin, N., Bargain, A., Launeau, P., 2010. Increase in seagrass distribution at Bourgneuf Bay (France) detected by spatial remote sensing. *Aquat. Bot.* 92, 185–194. <https://doi.org/10.1016/j.aquabot.2009.11.006>.
- Barsi, J.A., Lee, K., Kvaran, G., Markham, B.L., Pedelty, J.A., 2014. The spectral response of the Landsat-8 operational land imager. *Remote Sens.* 6, 10232–10251. <https://doi.org/10.3390/rs61010232>.
- Belgiu, M., Drăgu, L., 2016. Random forest in remote sensing: a review of applications and future directions. *ISPRS J. Photogramm. Remote Sens.* 114, 24–31. <https://doi.org/10.1016/j.isprsjprs.2016.01.011>.
- Benyoucef, I., Blandin, E., Lerouxel, A., Jesus, B., Rosa, P., Méléder, V., Launeau, P., Barillé, L., 2014. Microphytobenthos interannual variations in a north-European estuary (Loire estuary, France) detected by visible-infrared multispectral remote sensing. *Estuar. Coast. Shelf Sci.* 136, 43–52. <https://doi.org/10.1016/j.ecss.2013.11.007>.

- Bergsma, E.W.J., Almar, R., 2020. Coastal coverage of ESA Sentinel 2 mission. *Adv. Sp. Res.* 65, 2636–2644. <https://doi.org/10.1016/j.asr.2020.03.001>.
- Borja, A., Elliott, M., Andersen, J.H., Cardoso, A.C., Carstensen, J., Ferreira, J.G., Heiskanen, A.-S., Marques, J.C., Neto, J.M., Teixeira, H., Uusitalo, L., Uyarra, M.C., Zampoukas, N., 2013. Good Environmental Status of marine ecosystems: what is it and how do we know when we have attained it? *Mar. Pollut. Bull.* 76, 16–27. <https://doi.org/10.1016/j.marpolbul.2013.08.042>.
- Breiman, L., 2001. Random forests. *Mach. Learn.* 45, 5–32. <https://doi.org/10.1023/A:1010933404324>.
- Brito, A., Newton, A., Tett, P., Fernandes, T.F., 2010. Sediment and water nutrients and microalgae in a coastal shallow lagoon, Ria Formosa (Portugal): implications for the water framework directive. *J. Environ. Monit.* 12, 318–328. <https://doi.org/10.1039/b909429f>.
- Brito, A.C., Benyousef, I., Jesus, B., Brotas, V., Gernez, P., Mendes, C.R., Launeau, P., Dias, M.P., Barillé, L., 2013. Seasonality of microphytobenthos revealed by remote sensing in a South European estuary. *Cont. Shelf Res.* 66 <https://doi.org/10.1016/j.csr.2013.07.004>.
- Brotas, V., Cabrita, M.T., Portugal, A., Seródio, J., Catarino, F., 1995. Spatio-temporal distribution of the microphytobenthic biomass in intertidal flats of Tagus Estuary (Portugal). *Hydrobiologia* 300 (301), 93–104.
- Cartaxana, P., Ruivo, M., Hubas, C., Davidson, I., Seródio, J., Jesus, B., 2011. Physiological versus behavioral photoprotection in intertidal epipelagic and epipsammic benthic diatom communities. *J. Exp. Mar. Biol. Ecol.* 405 (1–2), 120–127. <https://doi.org/10.1016/j.jembe.2011.05.027>.
- Clarke, K.R., Warwick, R.M., 2001. *Change in Marine Communities: An Approach to Statistical Analysis and Interpretation*. Marine Laboratory, Plymouth, 2nd ed. PRIMER-E, Plymouth, UK.
- Cloern, J.E., 1987. Turbidity as a control on phytoplankton biomass and productivity in estuaries. *Cont. Shelf Res.* 7, 1367–1381.
- Colditz, R.R., 2015. An evaluation of different training sample allocation schemes for discrete and continuous land cover classification using decision tree-based algorithms. *Remote Sens.* 7, 9655–9681. <https://doi.org/10.3390/rs70809655>.
- Congalton, R.G., 1991. A review of assessing the accuracy of classifications of remotely sensed data. *Remote Sens. Environ.* 37, 35–46. [https://doi.org/10.1016/0034-4257\(91\)90048-B](https://doi.org/10.1016/0034-4257(91)90048-B).
- Consalvey, M., Paterson, D.M., Underwood, G.J.C., 2004. The ups and downs of life in a benthic biofilm: migration of benthic diatoms. *Diatom Res.* 19, 181–202. <https://doi.org/10.1080/0269249X.2004.9705870>.
- Daggers, T.D., Herman, P.M.J., van der Wal, D., Forster, R., 2020. Seasonal and spatial variability in patchiness of microphytobenthos on intertidal flats from sentinel-2 satellite imagery. *Front. Mar. Sci.* 7, 1–14. <https://doi.org/10.3389/fmars.2020.00392>.
- Daughtry, C.S.T., Walthall, C.L., Kim, M.S., Brown de Colstoun, E., McMurtrey III, J.E., 2000. Estimating corn leaf chlorophyll concentration from leaf and canopy reflectance. *Remote Sens. Environ.* 74, 229–239. <https://doi.org/10.3184/174751911X556684>.
- Drusch, M., Bello, U. Del, Carlier, S., Colin, O., Fernandez, V., Gascon, F., Hoersch, B., Isola, C., Laberinti, P., Martimort, P., Meygret, A., Spoto, F., Sy, O., Marchese, F., Bargellini, P., 2012. Sentinel-2: ESA's optical high-resolution mission for GMES operational services. *Remote Sens. Environ.* 120, 25–36. <https://doi.org/10.1016/j.rse.2011.11.026>.
- Du, G., Yan, H., Dupuy, C., 2017. Microphytobenthos as an indicator of environmental quality status in intertidal flats: case study of coastal ecosystem in Pertuis Charentais, France. *Estuar. Coast. Shelf Sci.* 196, 217–226. <https://doi.org/10.1016/j.ecss.2017.06.031>.
- Du, P., Samat, A., Waske, B., Liu, S., Li, Z., 2015. Random forest and rotation forest for fully polarized SAR image classification using polarimetric and spatial features. *ISPRS J. Photogramm. Remote Sens.* 105, 38–53. <https://doi.org/10.1016/j.isprsjprs.2015.03.002>.
- Duffy, J.P., Pratt, L., Anderson, K., Land, P.E., Shutler, J.D., 2018. Spatial assessment of intertidal seagrass meadows using optical imaging systems and a lightweight drone. *Estuar. Coast. Shelf Sci.* 200, 169–180. <https://doi.org/10.1016/j.ecss.2017.11.001>.
- Echappé, C., Gernez, P., Méléder, V., Jesus, B., Cognie, B., Decottignies, P., Sabbe, K., Barillé, L., 2018. Satellite remote sensing reveals a positive impact of living oyster reefs on microalgal biofilm development. *Biogeosciences* 15, 905–918. <https://doi.org/10.5194/bg-15-905-2018>.
- Elliott, M., Quintino, V., 2007. The estuarine quality paradox, environmental homeostasis and the difficulty of detecting anthropogenic stress in naturally stressed areas. *Mar. Pollut. Bull.* 54, 640–645. <https://doi.org/10.1016/j.marpolbul.2007.02.003>.
- European Commission, 2000. *Directive 2000/60/CE du Parlement européen et du Conseil du 23 octobre 2000 établissant un cadre pour une politique communautaire dans le domaine de l'eau*. *J. Off. des Communautés Eur.* du 22.12.2000 72 p.
- European Environment Agency, 2018. In: *European Waters Assessment of Status and Pressures*. <https://doi.org/10.4324/9780203938607>.
- Fairley, I., Mendzil, A., Togneri, M., Reeve, D.E., 2018. The use of unmanned aerial systems to map intertidal sediment. *Remote Sens.* 10 <https://doi.org/10.3390/rs10121918>.
- Fichot, C.G., Downing, B.D., Bergamaschi, B.A., Windham-Myers, L., Marvin-Dipasquale, M., Thompson, D.R., Gierach, M.M., 2016. High-resolution remote sensing of water quality in the San Francisco Bay-Delta Estuary. *Environ. Sci. Technol.* 50, 573–583. <https://doi.org/10.1021/acs.est.5b03518>.
- Frankenbach, S., Ezequiel, J., Plecha, S., Goessling, J.W., Vaz, L., Kühl, M., Dias, J.M., Vaz, N., Seródio, J., 2020. Synoptic spatio-temporal variability of the photosynthetic productivity of microphytobenthos and phytoplankton in a tidal estuary. *Front. Mar. Sci.* 7 <https://doi.org/10.3389/fmars.2020.00170>.
- Fyfe, S.K., 2003. Spatial and temporal variation in spectral reflectance: are seagrass species spectrally distinct? *Limnol. Oceanogr.* 48 (1 II), 464–479. [https://doi.org/10.4319/lo.2003.48.1\\_part\\_2.0464](https://doi.org/10.4319/lo.2003.48.1_part_2.0464).
- Georganos, S., Grippa, T., Vanhuyse, S., Lennert, M., Shimoni, M., Kalogirou, S., Wolff, E., 2018a. Less is more: optimizing classification performance through feature selection in a very-high-resolution remote sensing object-based urban application. *GISci. Remote Sens.* 55 (2), 221–242. <https://doi.org/10.1080/15481603.2017.1408892>.
- Georganos, S., Grippa, T., Vanhuyse, S., Lennert, M., Shimoni, M., Wolff, E., 2018b. Very high resolution object-based land use-land cover urban classification using extreme gradient boosting. *IEEE Geosci. Remote Sens. Lett.* 15 (4), 607–611. <https://doi.org/10.1109/LGRS.2018.2803259>.
- Ghosh, A., Fassnacht, F.E., Joshi, P.K., Kochb, B., 2014. A framework for mapping tree species combining hyperspectral and LiDAR data: role of selected classifiers and sensor across three spatial scales. *Int. J. Appl. Earth Obs. Geoinf.* 26, 49–63. <https://doi.org/10.1016/j.jag.2013.05.017>.
- Halpern, B.S., Walbridge, S., Selkoe, K.A., Kappel, C.V., Micheli, F., D'Agrosa, C., Bruno, J.F., Casey, K.S., Ebert, C., Fox, H.E., Fujita, R., Heinemann, D., Lenihan, H.S., Madin, E.M.P., Perry, M.T., Selig, E.R., Spalding, M., Steneck, R., Watson, R., 2008. A global map of human impact on marine ecosystems. *Science* 80 319, 948–952. <https://doi.org/10.1126/science.1149345>.
- Hammer, Ø., Harper, D.A.T., Ryan, P.D., 2001. *Past: paleontological statistics software package for education and data analysis*. *Palaentol. Electron.* 4, 178.
- Huete, A.R., 1988. A soil-adjusted vegetation index (SAVI). *Remote Sens. Environ.* 25, 295–309. [https://doi.org/10.1016/0034-4257\(88\)90106-X](https://doi.org/10.1016/0034-4257(88)90106-X).
- Kaufman, Y.J., Tanré, D., 1992. Atmospherically resistant vegetation index (ARVI) for EOS-MODIS. *IEEE Trans. Geosci. Remote Sens.* <https://doi.org/10.1109/36.134076>.
- Kelly, M., 2013. Data rich, information poor? Phytobenthos assessment and the water framework directive. *Eur. J. Phycol.* 48, 437–450. <https://doi.org/10.1080/09670262.2013.852694>.
- Kuhn, M., 2008. Building predictive models in R using the caret package. *J. Stat. Softw.* 28, 1–26. <https://doi.org/10.18637/jss.v028.i05>.
- Kulkarni, V.Y., Sinha, P.K., 2012. Pruning of random forest classifiers: a survey and future directions. In: *Proceedings – 2012 International Conference on Data Science and Engineering, ICDSE 2012*, pp. 64–68. <https://doi.org/10.1109/ICDSE.2012.6282329>.
- Kutser, T., Hedley, J., Giardino, C., Roelfsema, C., Brando, V.E., 2020. Remote sensing of shallow waters – a 50 year retrospective and future directions. *Remote Sens. Environ.* 240, 111619 <https://doi.org/10.1016/j.rse.2019.111619>.
- Launeau, P., Méléder, V., Verpoorter, C., Barillé, L., Kazempour-Ricci, F., Giraud, M., Jesus, B., Le Menn, E., 2018. Microphytobenthos biomass and diversity mapping at different spatial scales with a hyperspectral optical model. *Remote Sens.* 10, 716. <https://doi.org/10.3390/rs10050716>.
- Le Bris, A., Perrot, T., Liabot, P.-O., Cellier, L., Richier, S., 2019. Action 3 : Digitalisation du substrat sur l'ortholittorale V2. Etude comparative de l'évolution des habitats rocheux, sableux, vaseux incluant le schorre au moyen des orthos littorales V1 et V2 acquises sur les masses d'eau de la façade Manche-Atlantique. CEVA. pp. 22.
- Legendre, P., Legendre, L., 1998. *Numerical Ecology*. Elsevier.
- Liu, H.Q., Huete, A., 1995. Feedback based modification of the NDVI to minimize canopy background and atmospheric noise. *IEEE Trans. Geosci. Remote Sens.* 33, 457–465. <https://doi.org/10.1109/36.377946>.
- MacIntyre, H.L., Geider, R.J., Miller, D.C., 1996. Microphytobenthos: The Ecological Role of the "Secret Garden" of Unvegetated, Shallow-Water Marine Habitats. I. Distribution, Abundance and Primary Production. *Estuaries* 19, 186–201.
- Main-Knorn, M., Pflug, B., Louis, J., Debaecker, V., Müller-Wilm, U., Gascon, F., 2017. *Sen2Cor for Sentinel-2 3* <https://doi.org/10.1117/12.2278218>.
- Mantas, V.M., Pereira, A.J.S.C., Neto, J., Patrício, J., Marques, J.C., 2013. Monitoring estuarine water quality using satellite imagery. The Mondego river estuary (Portugal) as a case study. *Ocean Coast. Manage.* 72, 13–21. <https://doi.org/10.1016/j.ocecoaman.2011.06.013>.
- Martin, R.D., 2020. *Determining estuarine seagrass condition measures from low altitude multi-spectral imagery flown by remote piloted aircraft* (Ph.D. thesis). University of Waikato, p. 342.
- McFeeters, S.K., 1996. The use of the normalized difference water index (NDWI) in the delineation of open water features. *Int. J. Remote Sens.* 17, 1425–1432. <https://doi.org/10.1080/01431169608948714>.
- McLusky, D.D., Elliott, M., 2004. *The estuarine ecosystem: ecology, threats, and management*. New York Oxford Univ. Press 223. <https://doi.org/10.1093/ISBN>.
- Méléder, Barillé, L., Launeau, P., Carrière, V., Rincé, Y., 2003b. Spectrometric constraint in analysis of benthic diatom biomass using monospecific cultures. *Remote Sens. Environ.* 88, 386–400. <https://doi.org/10.1016/j.rse.2003.08.009>.
- Méléder, V., Barillé, L., Rincé, Y., Morancas, M., Rosa, P., Gaudin, P., 2005. Spatio-temporal changes in microphytobenthos structure analysed by pigment composition in a macrotidal flat (Bourgneuf Bay, France). *Mar. Ecol. Prog. Ser.* 297, 83–99.
- Méléder, Launeau, P., Barillé, L., Rincé, Y., 2003a. Cartographie des peuplements du microphytobenthos par télédétection spatiale visible-infrarouge dans un écosystème microbenthique. *C. R. Biol.* 326, 377–389. [https://doi.org/10.1016/S1631-0691\(03\)00125-2](https://doi.org/10.1016/S1631-0691(03)00125-2).
- Ménesguen, A., Dussauze, M., Dumas, F., 2018. Designing optimal scenarios of nutrient loading reduction in a WFD/MSFD perspective by using passive tracers in a biogeochemical-3D model of the English Channel/Bay of Biscay area. *Ocean Coast. Manage.* 163, 37–53. <https://doi.org/10.1016/j.ocecoaman.2018.06.005>.
- Merrifield, M.S., Hines, E., Liu, X., Beck, M.W., 2011. Building regional threat-based networks for estuaries in the Western United States. *PLoS One* 6. <https://doi.org/10.1371/journal.pone.0017407>.

- Monbet, Y., 1992. Control of phytoplankton biomass in estuaries: a comparative analysis of microtidal and macrotidal estuaries. *Estuaries* 15, 563–571. <https://doi.org/10.2307/1352398>.
- Morelle, J., Clauquin, P., Orvain, F., 2020. Evidence for better microphytobenthos dynamics in mixed sand/mud zones than in pure sand or mud intertidal flats (Seine estuary, Normandy, France). *PLoS One* 15 (8), e0237211. <https://doi.org/10.1371/journal.pone.0237211>.
- Muller-Karger, F.E., Hestir, E., Ade, C., Turpie, K., Roberts, D.A., Siegel, D., Miller, R.J., Humm, D., Izenberg, N., Keller, M., Morgan, F., Frouin, R., Dekker, A.G., Gardner, R., Goodman, J., Schaeffer, B., Franz, B.A., Pahlevan, N., Mannino, A.G., Concha, J.A., Ackleson, S.G., Cavanaugh, K.C., Romanou, A., Tzortziou, M., Boss, E.S., Pavlick, R., Freeman, A., Rousseaux, C.S., Dunne, J., Long, M.C., Klein, E., McKinley, G.A., Goes, J., Letelier, R., Kavanaugh, M., Roffer, M., Bracher, A., Arriago, K.R., Dierssen, H., Zhang, X., Davis, F.W., Best, B., Guralnick, R., Moisan, J., Sosik, H.M., Kudela, R., Mouw, C.B., Barnard, A.H., Palacios, S., Roesler, C., Drakou, E.G., Appeltans, W., Jetz, W., 2018. Satellite sensor requirements for monitoring essential biodiversity variables of coastal ecosystems. *Ecol. Appl.* 28, 749–760. <https://doi.org/10.1002/eap.1682>.
- Murphy, R.J., Tolhurst, T.J., Chapman, M.G., Underwood, A.J., 2008. Spatial variation of chlorophyll in estuarine mudflats determined by field-based remote sensing. *Mar. Ecol. Prog. Ser.* 365, 45–55. <https://doi.org/10.3354/meps07456>.
- Murray, N.J., Phinn, S.R., DeWitt, M., Ferrari, R., Johnston, R., Lyons, M.B., Clinton, N., Thau, D., Fuller, R.A., 2019. The global distribution and trajectory of tidal flats. *Nature* 565, 222–225. <https://doi.org/10.1038/s41586-018-0805-8>.
- Oh, S.H., Koh, C.H., 1995. Distribution of diatoms in the surficial sediments of the Mangyung-Dongjin tidal flat, west coast of Korea (Eastern Yellow Sea). *Mar. Biol.* 122, 487–496. <https://doi.org/10.1007/BF00350883>.
- Orvain, F., Lefebvre, S., Montepini, J., Sébire, M., Gangnery, A., Sylvand, B., 2012. Spatial and temporal interaction between sediment and microphytobenthos in a temperate estuarine macro-intertidal bay. *Mar. Ecol. Prog. Ser.* 458, 53–68. <https://doi.org/10.3354/meps09698>.
- Papathanasopoulou, E., Simis, S., Alikas, K., Ansper, A., Anttila, S., Jenni, A., Barillé, A.-L., Barillé, L., Brando, V., Bresciani, M., Bučas, M., Gernez, P., Giardino, C., Harin, N., Hommersom, A., Kangro, K., Kaupilla, P., Koponen, S., Laanen, M., Neil, C., Papadakis, D., Peters, S., Poikane, S., Kathrin Poser, K., Pires, M.D., Riddick, C., Spyros, E., Tyler, A., Vaićević, D., Warren, M., Zoffoli, M.L., 2019. In: Satellite-assisted Monitoring of Water Quality to Support the Implementation of the Water Framework Directive EOMORES White Paper. 28. <https://doi.org/10.5281/zenodo.3463051>.
- Park, J., Kwon, B.O., Kim, M., Hong, S., Ryu, J., Song, S.J., Khim, J.S., 2014. Microphytobenthos of Korean tidal flats: a review and analysis on floral distribution and tidal dynamics. *Ocean Coast. Manage.* 102, 471–482. <https://doi.org/10.1016/j.ocecoaman.2014.07.007>.
- Paterson, D.M., Hagerthey, S.E., 2001. *Microphytobenthos in contrasting coastal ecosystems: biology and dynamics*. In: Reize, K. (Ed.), *Ecological Comparisons of Sedimentary Shores*. Springer-Verlag, Berlin, pp. 105–125.
- Perrot, T., Rossi, N., Ménesguen, A., Dumas, F., 2014. Modelling green macroalgal blooms on the coasts of Brittany, France to enhance water quality management. *J. Mar. Syst.* 132, 38–53. <https://doi.org/10.1016/j.jmarsys.2013.12.010>.
- Poursanis, D., Topouzelis, K., Chrysoulakis, N., 2018. Mapping coastal marine habitats and delineating the deep limits of the Neptune's seagrass meadows using very high resolution Earth observation data. *Int. J. Remote Sens.* 39, 8670–8687. <https://doi.org/10.1080/01431161.2018.1490974>.
- Prygiel, J., Coste, M., 1993. The assessment of water quality in the Artois-Picardie water basin (France) by the use of diatom indices. *Hydrobiologia* 269–270, 343–349. <https://doi.org/10.1007/BF00028033>.
- Ratmaya, W., Soudant, D., Salmon-Monviola, J., Cochenne-Laureau, N., Goubert, E., Andrieux-Loyer, F., Barillé, L., Souchu, P., 2018. Reduced phosphorus loads from the Loire and Vilaine Rivers were accompanied by increasing eutrophication in Vilaine Bay (South Brittany, France). *Biogeosci.* 1–29. <https://doi.org/10.5194/bg-2018-406>.
- Riaux-Gobin, C., 1985. Long-term changes in microphytobenthos in a Brittany estuary after the “Amoco Cadiz” oil spill. *Mar. Ecol. Prog. Ser.* 24, 51–56.
- Ribeiro, L., Brotas, V., Hernández-Fariñas, T., Jesus, B., Barillé, L., 2020. Assessing alternative microscopy-based approaches to species abundance description of intertidal diatom communities. *Front. Mar. Sci.* 7. <https://doi.org/10.3389/fmars.2020.00036>.
- Ribeiro, L., Le Bris, A., Hernández Fariñas, T., Buchet, R., Dutertre, M., Metzger, E., Rosa, P., Gernez, P., Lerouxel, A., Barillé, L., 2018. Étude de la pertinence du suivi des peuplements du microphytobenthos estuarien. Rapport d'étude pour l'Agence Française de la Biodiversité. AFB. <https://doi.org/10.5281/zenodo.3723043>.
- Roelfsema, C.M., Lyons, M., Kovacs, E.M., Maxwell, P., Saunders, M.I., Samper-Villarreal, J., Phinn, S.R., 2014. Multi-temporal mapping of seagrass cover, species and biomass: a semi-automated object based image analysis approach. *Remote Sens. Environ.* 150, 172–187. <https://doi.org/10.1016/j.rse.2014.05.001>.
- Rouse, J.W., Hass, R.H., Schell, J.A., Deering, D.W., 1973. Monitoring vegetation systems in the great plains with ERTS. *Third Earth Resour. Technol. Satell. Symp.* 1, 309–317.
- Saburova, M.A., Polikarpov, I.G., Burkovsky, I.V., 1995. Spatial structure of an intertidal sandflat microphytobenthic community as related to different spatial scales. *Mar. Ecol. Prog. Ser.* 129, 229–239.
- Savelli, R., Dupuy, C., Barillé, L., Lerouxel, A., Guizien, K., Philippe, A., Bocher, P., Polsenaere, P., Le Fouest, V., 2018. On biotic and abiotic drivers of the microphytobenthos seasonal cycle in a temperate intertidal mudflat: a modelling study. *Biogeosciences* 15, 7243–7271. <https://doi.org/10.5194/bg-15-7243-2018>.
- Schaeffer, B.A., Myer, M.H., 2020. Resolvable estuaries for satellite derived water quality within the continental United States. *Remote Sens. Lett.* 11, 535–544. <https://doi.org/10.1080/2150704X.2020.1717013>.
- Spilmont, N., Davoult, D., Migné, A., 2006. Benthic primary production during emersion: in situ measurements and potential primary production in the Seine Estuary (English Channel, France). *Mar. Pollut. Bull.* 53, 49–55. <https://doi.org/10.1016/j.marpolbul.2005.09.016>.
- Spilmont, N., Seuront, L., Meziane, T., Welsh, D.T., 2011. There's more to the picture than meets the eye: sampling microphytobenthos in a heterogeneous environment. *Estuar. Coast. Shelf Sci.* 95, 470–476. <https://doi.org/10.1016/j.ecss.2011.10.021>.
- Stevenson, R.J., 1997. Scale-dependent determinants and consequences of source. *J. North Am. Benthol. Soc.* 16, 248–262.
- Stevenson, R.J., Pan, Y., Van Dam, H., 2010. *Assessing ecological conditions in rivers and streams with diatoms*. In: Stoermer, E.F., Smol, J.P. (Eds.), *The Diatoms: Applications to the Environmental and Earth Sciences*. Cambridge University Press, Cambridge, pp. 57–85.
- Thanh Noi, P., Kappas, M., 2017. Comparison of random forest, k-nearest neighbor, and support vector machine classifiers for land cover classification using sentinel-2 imagery. *Sensors* 18, 18. <https://doi.org/10.3390/s18010018>.
- Traganos, D., Reinartz, P., 2018a. Interannual change detection of mediterranean seagrasses using RapidEye image time series. *Front. Plant Sci.* 9, 1–15. <https://doi.org/10.3389/fpls.2018.00096>.
- Traganos, D., Reinartz, P., 2018b. Mapping Mediterranean seagrasses with Sentinel-2 imagery. *Mar. Pollut. Bull.* 134, 197–209. <https://doi.org/10.1016/j.marpolbul.2017.06.075>.
- Trobajo, R., Sullivan, M.J., 2010. Applied diatom studies in estuaries and shallow coastal environments. In: *The Diatoms: Applications for the Environmental and Earth Sciences*, second ed. Cambridge University Press, pp. 309–323. <https://doi.org/10.1017/CBO9780511763175.017>.
- Tucker, C.J., 1979. Red and photographic infrared linear combinations for monitoring vegetation. *Remote Sens. Environ.* 8, 127–150. [https://doi.org/10.1016/0034-4257\(79\)90013-0](https://doi.org/10.1016/0034-4257(79)90013-0).
- Underwood, G.J.C., Kromkamp, J., 1999. Primary production by phytoplankton and microphytobenthos in estuaries. *Adv. Ecol. Res.* 29, 93–153.
- van der Wal, D., Wielemaker-van den Dool, A., Herman, P.M.J., 2010. Spatial synchrony in intertidal benthic algal biomass in temperate coastal and estuarine ecosystems. *Ecosystems* 13, 338–351. <https://doi.org/10.1007/s10021-010-9322-9>.
- Vetrivel, A., Gerke, M., Kerle, N., Vosselman, G., 2015. Identification of damage in buildings based on gaps in 3D point clouds from very high resolution oblique airborne imagery. *ISPRS J. Photogramm. Remote Sens.* 105, 61–78. <https://doi.org/10.1016/j.isprsjprs.2015.03.016>.
- Vieira, S., Cartaxana, P., Máguas, C., Da Silva, J.M., 2016. Photosynthesis in estuarine intertidal microphytobenthos is limited by inorganic carbon availability. *Photosynth. Res.* 128 (1), 85–92. <https://doi.org/10.1007/s1120-015-0203-0>.
- Villoslada, M., Bergamo, T.F., Ward, R.D., Burnside, N.G., Joyce, C.B., Bunce, R.G.H., Sepp, K., 2020. Fine scale plant community assessment in coastal meadows using UAV based multispectral data. *Ecol. Indic.* 111, 105979. <https://doi.org/10.1016/j.ecolind.2019.105979>.
- Wang, X., Xiao, X., Zou, Z., Chen, B., Ma, J., Dong, J., Doughty, R.B., Zhong, Q., Qin, Y., Dai, S., Li, X., Zhao, B., Li, B., 2018. Tracking annual changes of coastal tidal flats in China during 1986–2016 through analyses of Landsat images with Google Earth Engine. *Remote Sens. Environ.* <https://doi.org/10.1016/j.rse.2018.11.030>.
- Weerman, E.J., Herman, P.M.J., Van de Koppel, J., 2011. Top-down control inhibits spatial self-organization of a patterned landscape. *Ecology* 92, 487–495. <https://doi.org/10.1890/10-0270.1>.
- Wright, M.N., Ziegler, A., 2017. Ranger: A Fast Implementation of Random Forests for High Dimensional Data in C++ and R. *J. Stat. Softw.* 77, 1–17. <https://doi.org/10.18637/jss.v077.i01>.
- Zhang, C., 2015. Applying data fusion techniques for benthic habitat mapping and monitoring in a coral reef ecosystem. *ISPRS J. Photogramm. Remote Sens.* 104, 213–223. <https://doi.org/10.1016/j.isprsjprs.2014.06.005>.
- Zhang, L., Suganthan, P.N., 2014. Random forests with ensemble of feature spaces. *Pattern Recogn.* 47, 3429–3437. <https://doi.org/10.1016/j.patcog.2014.04.001>.
- Zhong, Z., Li, Y., Han, Z., Yang, Z., 2020. Ship Target Detection Based on LightGBM Algorithm 425–429. <https://doi.org/10.1109/cibda50819.2020.00102>.
- Zoffoli, L., Gernez, P., Rosa, P., Le Bris, A., Brando, V.E., Barillé, A.L., Harin, N., Peters, S., Poser, K., Spaias, L., Peralta, G., Barillé, L., 2020. Sentinel-2 remote sensing of *Zostera noltei*-dominated intertidal seagrass meadows. *Remote Sens. Environ.* 251, 112020. <https://doi.org/10.1016/j.rse.2020.112020>.